Earth and Planetary Science Letters 281 (2009) 258–266

Contents lists available at ScienceDirect

Earth and Planetary Science Letters

journal homepage: www.elsevier.com/locate/epsl

Spectral, mineralogical, and geochemical variations across Home Plate, Gusev Crater, Mars indicate high and low temperature alteration

M.E. Schmidt [a,*], W.H. Farrand [b], J.R. Johnson [c], C. Schröder [d], J.A. Hurowitz [e], T.J. McCoy [a], S.W. Ruff [f], R.E. Arvidson [g], D.J. Des Marais [h], K.W. Lewis [i], D.W. Ming [j], S.W. Squyres [k], P.A. de Souza Jr. [l]

[a] Dept. of Mineral Sciences, Smithsonian Institution, Washington, DC 20560, United States
[b] Space Science Institute, Boulder, Colorado 80301, United States
[c] Astrogeology Team, United States Geological Survey, Flagstaff, Arizona 86001, United States
[d] Institut für Anorganische Chemie und Analytische Chemie, Johannes Gutenberg Universität, D-55128 Mainz, Germany
[e] Jet Propulsion Laboratory, California Institute of Technology, Pasadena, CA 91109, United States
[f] School of Earth and Space Exploration, Arizona State University, Tempe, AZ 85287, United States
[g] Dept. of Earth and Planetary Sciences, Washington University, St. Louis, MO 63130, United States
[h] Exobiology Branch, NASA Ames Research Center, Moffett Field, CA 94035, United States
[i] Division of Geological and Planetary Sciences, California Institute of Technology, Pasadena, CA 91125, United States
[j] NASA Johnson Space Center, Houston, TX 77058, United States
[k] Dept. of Astronomy, Space Sciences Bldg., Cornell University, Ithaca, NY 14853, United States
[l] Tasmanian ICT Center, CSIRO, Hobart, TAS 7000, Australia

ARTICLE INFO

Article history:
Received 16 October 2008
Received in revised form 20 February 2009
Accepted 23 February 2009
Available online 26 March 2009

Editor: R.W. Carlson

Keywords:
Mars geology
Gusev Crater
hydrothermal alteration

ABSTRACT

Over the last ~3 years in Gusev Crater, Mars, the Spirit rover observed coherent variations in color, mineralogy, and geochemistry across Home Plate, an ~80 m-diameter outcrop of basaltic tephra. Observations of Home Plate from orbit and from the summit of Husband Hill reveal clear differences in visible/near-infrared (VNIR) colors between its eastern and western regions that are consistent with mineralogical compositions indicated by Mössbauer spectrometer (MB) and by Miniature Thermal Emission Spectrometer (Mini-TES). Pyroxene and magnetite dominate the east side, while olivine, nanophase Fe oxide (npOx) and glass are more abundant on the western side. Alpha Particle X-Ray Spectrometer (APXS) observations reveal that eastern Home Plate has higher Si/Mg, Al, Zn, Ni, and K, while Cl and Br are higher in the west. We propose that these variations are the result of two distinct alteration regimes that may or may not be temporally related: a localized, higher temperature recrystallization and alteration of the east side of Home Plate and lower temperature alteration of the western side that produced npOx.

Published by Elsevier B.V.

1. Introduction

In order to maximize discovery when the Mars Exploration Rover Spirit first landed in Gusev Crater in 2004, a reconnaissance traverse was conducted that rarely doubled back. But over the last three of its five years on Mars, Spirit has completed a circumnavigation of Home Plate (Fig. 1; Arvidson et al., 2008), an ~80 m-diameter platform of basaltic pyroclastic layered deposits that were variably reworked by eolian processes (Fig. 2; Squyres et al., 2007). During its traverse, observations made by Spirit reveal coherent changes in spectral characteristics, mineralogy, and composition that are consistent with alteration gradients across the Home Plate outcrop. The extended traverse around Home Plate made it possible to perform a systematic, integrated study of this gradient across the structure.

Both the Spirit and Opportunity rovers have examined rocks that indicate diverse alteration conditions at their landing sites, including variable water/rock ratios, pH and temperatures (e.g., Haskin et al., 2005; Tosca et al., 2005; Hurowitz et al., 2006; Ming et al., 2008). In the Home Plate region (Fig. 1), Spirit encountered a suite of rocks and soils that implicate volcanism and hydrothermal activity (e.g., Squyres et al., 2007; Schmidt et al., 2008; Morris et al., 2008). For example, opalline silica deposits in the Eastern Valley (Fig. 1) formed by either intense acid-vapor alteration of a volcanic protolith or sinter precipitation from silica-saturated aqueous fluids (Squyres et al., 2008). To the north and to the southeast (Tyrone; Fig. 1) are hydrated sulfate soils of likely fumarolic or hydrothermal origin (Yen et al., 2008). At Low Ridge (Fig. 1), rocks have abundant hematite, high K and/or Zn and were probably affected by hydrothermal alteration (Ming et al., 2008; Morris et al., 2008). This study of the mineralogical and compositional gradient across Home Plate is in the context of a once dynamic hydrothermal system and allows us to constrain reactions and conditions over a known distance and to envision fluid flow in the subsurface of Mars.

* Corresponding author.
E-mail address: schmidtm@si.edu (M.E. Schmidt).

0012-821X/$ – see front matter. Published by Elsevier B.V.
doi:10.1016/j.epsl.2009.02.030

2. The Home Plate traverse

Spirit performed *in situ* geochemical and mineralogical observations of Home Plate at five locations (Fig. 1) over sols 749 to ~1500 (1 sol = 1 martian day). At the northwest (Barnhill; Fig. 2A) and east (Pesapallo; Fig. 2B) scarps, several targets were selected along 1–2 m stratigraphic sections. Elsewhere, Spirit examined the upper surface of Home Plate (Texas Chili, Pecan Pie, and Chanute; Arvidson et al., 2008).

The Home Plate edifice is mainly constructed of a fine-grained, cross-bedded and laminated unit, but at its northwest corner (Barnhill, Fig. 2A) and in the northern Eastern Valley (Fig. 1A), a lower, more coarsely bedded, coarser-grained unit is exposed. The interpretation that pyroclastic and likely hydrovolcanic processes constructed Home Plate is based on textures that include graded beds, an apparent bomb sag and possible accretionary lapilli in the lower unit (Squyres et al., 2007; Lewis et al., 2008). Compositional characteristics, including volatile element enrichments indicate that a hydrothermal chloride brine interacted with the deposit (Schmidt et al., 2008). Cross-bedding and sorting in the upper part of Home Plate reflect either eolian reworking or primary base surge deposition. Beds that make up Home Plate dip 0–35° toward its center, apparently draping a pre-existing circular depression, such as a small impact crater (Squyres et al., 2007; Lewis et al., 2008). The eastern rim is 4.4 m higher than the west (Schröder et al., 2008) and this most likely reflects either draping of underlying topography or later deformation. Eastern and southeastern Home Plate are linked stratigraphically by tracing a conspicuous erosion-resistant doublet marker layer (Fig. 2B) that occurs at the base of the Pesapallo section and extends southward around the east side to underlie Texas Chili. Resistant doublet layers on the east side of Home Plate correlate with those situated between the lower and upper units of the Barnhill section on the northwest side (Fig. 2A); they share similar thicknesses, morphologies, and stratigraphic positions at the base of the cross bedded unit (Lewis et al., 2008).

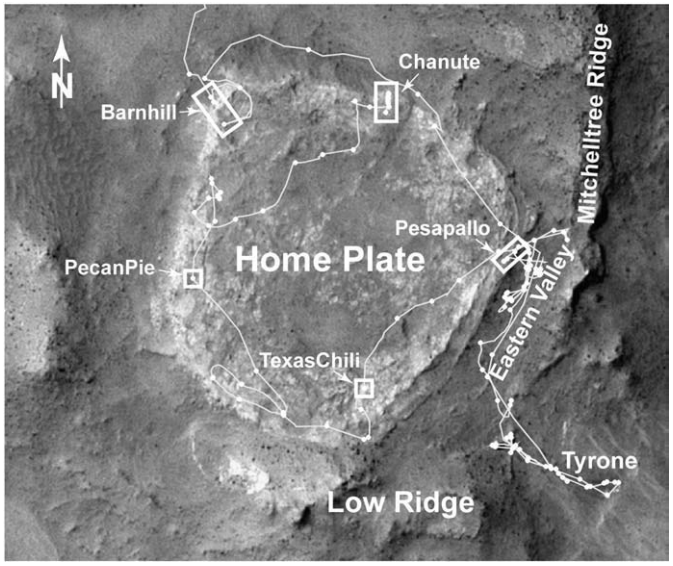

Fig. 1. A: Orbital HiRISE (High Resolution Imaging Science Experiment) images of Home Plate PSP_005456_1650 (collected 9/25/07). Thin white line denotes Spirit's traverse (Arvidson et al., 2008). Locations of targets are indicated.

3. Results

We present observations made by the High Resolution Imaging Science Experiment (HiRISE) camera onboard the Mars Reconnaissance Orbiter (MRO; McEwen et al., 2007) and the instruments of the Athena Payload on Spirit (Squyres et al., 2003). In particular, we include results of multispectral imaging by the Panoramic Camera (Pancam) and analyses by the MB, which determines Fe-bearing minerals (Table 1); the Mini-TES, which assesses mineralogy remotely based on emissivity spectra (Table 2); and the APXS, which analyzes major and some minor element concentrations (Table 3). Wherever possible, the Rock Abrasion Tool (RAT) brush cleared dust from rock targets prior to analysis.

3.1. Multispectral observations

Color differences across Home Plate are visible in observations made by the orbital HiRISE camera, such as a false color composite (Fig. 3A) illustrating the near-infrared (874 nm), red (694 nm), and blue-green (536 nm) channels. Colors are exaggerated in a decorrelation stretch of the HiRISE subscene (Fig. 3B) where the surrounding basalt sand-covered plains are mostly blue, surfaces on the western rim of Home Plate are yellow-orange and the center and eastern rim of Home Plate are mottled blue-green to green. Some of these color differences are also highlighted in the composite of fraction images (Fig. 3C) derived from spectral mixture analysis (Adams et al., 1993) of the three color data. Bright dust or bright colored surfaces in the fraction image are red, basaltic sands or spectrally similar materials are in green and shaded surfaces are blue. The western rim is red, indicating a higher fraction of dust and/or bright colored surfaces. Parts of the eastern rim and southeastern quadrant of Home Plate have higher proportions of the "basaltic sands" fraction image, indicating either greater amounts of basaltic sands or the indurated basaltic clasts that make up the Home Plate outcrop.

Looking south from the summit of Husband Hill (0.7 km to the north) on sol 595, Pancam obtained multispectral images of Home Plate. A RGB false-color composite (using 753, 535, and 432 nm bands; Fig. 4A) reveals a dichotomy between the east (blue/green-toned) and west (red-toned) portions of Home Plate, consistent with HiRISE images collected on Spirit's sol 1325 (Fig. 3). The color differences indicate that the eastern portion of Home Plate is not as contaminated by airfall dust as the western edge and/or that the materials comprising the uppermost eastern surface are less oxidized (thus "bluer"). Pancam color scenes taken on top of Home Plate confirm higher red/blue ratios towards the west. Extensive imaging since sol 1477 from the north side of Home Plate is consistent with these observations, although additional analyses are ongoing.

The spectral properties of dust-free rock surfaces were evaluated for RAT brushed rock targets. Corresponding Microscopic Imager (MI) images confirm near complete removal of dust grains>0.1 mm. Pancam spectra of RAT brush spots indicate that rock surfaces in the western part of Home Plate have greater 535 nm band depths and shallower (less negative) 601 nm band depths than in the east (Fig. 5). Band depths at 535 nm tend to correlate with Fe^{3+}/Fe_{Total} in Gusev rocks measured by the MB, possibly due to the relative abundance of finely crystalline red hematite (Farrand et al., 2006, 2008). Differences in the 601 nm band depth can be influenced either by the ratio of pyroxene/olivine or by the presence of goethite, although MB did not detect goethite in these materials (Table 1). Because clear spectral differences have been detected in dust-free rock surfaces, surficial dust deposits are unlikely to be the dominant cause of the persistent color dichotomy. Variations in spectral parameters across Home Plate verify that color contrasts observed at greater distances reflect meaningful differences in outcrop mineralogy.

3.2. Mineralogy

At both the eastern and northwestern sides of Home Plate, there is little internal mineralogical variability among the multiple targets

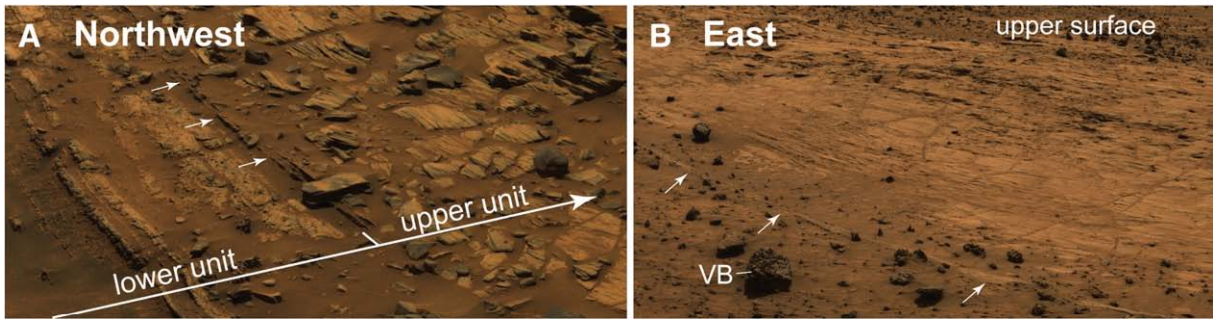

Fig. 2. Pancam images of the edges of Home Plate. Marker doublet layer is indicated by arrows. A: Subset of Gibson Panorama at the northwest corner of Home Plate near the Barnhill section. B: Subset of Ballpark Panorama of east Home Plate near the Pesapallo section (c.f. http://marswatch.astro.cornell.edu/pancam_instrument/mosaics.html). Example vesicular basalt is indicated by VB.

acquired along the two stratigraphic traverses. However, the two sides are mineralogically distinct. MB observations indicate that Fe in the Barnhill section is almost equally distributed between npOx, pyroxene, magnetite and olivine, whereas the Fe of the Pesapallo section occurs dominantly in magnetite (up to 54%) and pyroxene with lesser amounts in npOx, hematite, and olivine (Fig. 4C; Table 1). The Fe-bearing mineralogy determined by MB is reported as component subspectral areas, which reflect the quantitative distribution of Fe between mineral phases. Subspectral areas can be recast into wt.% using, for example, the procedure outlined by McSween et al. (2008). Ranges in Fe concentration found by APXS for targets within the upper cross-bedded unit are equivalent within error (15.5–16.8 in east vs. 15.4–16.9 in west; Table 3). Across the upper surface of Home Plate, MB olivine subspectral areas increase steadily from east to west–northwest (Figs. 4C and 6A and B). The sum of olivine and pyroxene subspectral areas is nearly constant in the Barnhill and Pesapallo section rocks (Fig. 6C), but is notably lower in the targets Chanute and Pecan Pie. The abundant magnetite at Home Plate may constrain the fO_2 during its formation to at or above the quartz–fayalite–magnetite (QFM) buffer. Higher hematite contents in Chanute and Pecan Pie (14 and 18% subspectral area, respectively) might reflect alteration of the Fe-silicate phases. From east to west–northwest, npOx increases as a step (Fig. 6B); 6–11% of the Fe in the Pesapallo targets and 26–31% of the Fe in other Home Plate targets are contained in npOx.

Remote observations of rock surfaces by Mini-TES also reveal differences between the Barnhill and Pesapallo sections (Table 2) with no significant intra-section variation. Deconvolutions of Mini-TES spectra indicate that pyroxene contents increases to the east, consistent with MB measurements. The difference in olivine contents across Home Plate from Mini-TES deconvolutions is not significant within error (10% in west vs. 5% in east ±5%; Table 3) and this most likely reflects detection limits of the instrument. A component modeled as basaltic glass is dominant in the Barnhill section (northwest), but is less important in the Pesapallo section (east). The component consistent with a primary volcanic glass may instead represent devitrified glass or an unknown amorphous secondary silicate. Other secondary silicates that are spectrally similar to phyllosilicate and zeolite phases are also modeled (up to 25%) in western Home Plate rocks. A sulfate component (20%) is detected on the eastern side of Home Plate that is not supported by S concentrations found by APXS (Table 3). The sulfate component most likely reflects contamination by surface dust as has been described elsewhere in Gusev Crater (Ruff et al., 2006). Magnetite was not detected in Mini-TES deconvolutions despite its inclusion in the spectral library because some of its spectral features are longward of its bandpass and other features are obscured by the atmospheric CO_2 band (Squyres et al., 2007).

3.3. Geochemistry

The composition of Home Plate is alkali-rich basalt (45–47% SiO_2, Table 3), similar to nearby vesicular basalts (Schmidt et al., 2008). Targets from the upper cross-bedded unit exhibit similar concentrations of elements that partition strongly into magnetite (Fe, Ti, Cr, Mn; Fig. 7A; Table 3). In contrast, the lower Barnhill targets have lower Ti and higher Fe that most likely reflect real stratigraphic differences because undisturbed soils and dust tend to have lower Fe (Fig. 7A). Absolute differences are small (~1 wt.%), but Si/Mg and Al tend to be higher in the east, while Ca tends to be higher in the west (Fig. 7B–C

Table 1
Mössbauer areas for component subspectra and Fe^{3+}/Fe_{Total}.

Section	Barnhill_Ace	Posey_Manager	JamesCool PapaBell_Stars	Pecan Pie	Chanute	Texas Chili	Pesapallo	June Emerson	Elizabeth Emery	Esperanza_Palma
	Barnhill	Barnhill	Barnhill		Chanute		Pesapallo	Pesapallo	Pesapallo	basalt
Unit	Lower unit northwest	Upper unit northwest	Upper sfc. northwest	Upper sfc. west	Upper sfc. north	Upper sfc. south	Upper unit east	Upper unit east	Upper sfc. east	Low ridge
Sol	748	754	762	1370	1411	1328	1207	1213	1217	1056
Type	Unbrushed	Brushed	Brushed	Brushed	Brushed	Brushed	Brushed	Brushed	Brushed	Unbrushed
Ol %	18	17	17	12	9	4	1	2	2	4
Px %	22	23	23	15	22	30	41	37	38	45
npOx %	29	27	29	31	31	25	11	6	8	4
Mt %	24	31	28	29	29	34	42	54	51	45
Hm %	7	3	3	14	9	7	5	1	1	1
Fe^{3+}/Fe_{Total}	0.53	0.53	0.52	0.64	0.62	0.56	0.48	0.44	0.46	0.40

Ilmenite, chromite, sulfates, and garnet were not detected by Mössbauer spectrometer in any of these rocks. Uncertainty in subspectral areas is ±2%. Uncertainty for Fe^{3+}/Fe_{Total} is ±0.03. A more complete summary of these data are presented by Morris et al. (2008).

Table 2
Average Mini-TES spectral deconvolution results for the Barnhill and Pesapallo sections of Home Plate.

	Barnhill (Northwest)	Pesapallo (East)
Basaltic glass	40	20
Secondary silicates	25	5
Plagioclase	10	10
Olivine	10	5
Pyroxene	5	35
Sulfate	5	20

Values are normalized to 100% and rounded to the nearest 5%. Error is approximately ±5%. Deconvolution routine is presented by Ruff et al. (2006) with a mirror dust correction by Smith et al. (2006). Secondary silicates may represent phyllosilicate or zeolite phases. Representative Mini-TES spectra are available in the online electronic supplement.

Table 3). Elements more susceptible to alteration (Fig. 7C–D) exhibit noticeable (>100 ppm) aerographic variations; Zn, Ni, and K concentrations are higher in the east, whereas Cl and Br concentrations are higher in the west. Texas Chili has high concentrations of Cl, Br, Zn, and K, (Fig. 7C–D; Table 3), possibly reflecting its intermediate east–west position (Fig. 1A). Undisturbed Gusev soil analyses represent the best-guess compositional range for dust contamination. These soils have less Zn than eastern Home Plate targets and less Cl and Br than those from the west, indicating that a dust coating did not cause the geochemical variations across Home Plate.

4. A confluence of observations

Observations made over two years by multiple instruments consistently indicate that the east and west sides of Home Plate are

Table 3
Elemental compositions of Home Plate rocks, Gusev Crater.

Target name	Barnhill_ Ace	Barnhill_Fastball	Posey_Manager	CoolPapaBell_ Stars	CoolPapaBell_ Crawford	Pecan Pie	Chanute_Brushed1	Chanute_Brushed2	Freeman_Brushed1
Section	Barnhill	Barnhill	Barnhill	Barnhill	Barnhill		Chanute	Chanute	Chanute
Location	Lower unit northwest HP	Lower unit northwest HP	Upper unit northwest HP	Upper sfc. northwest HP	Upper sfc. northwest HP	Upper sfc. west HP	Upper sfc. north HP	Upper sfc. north HP	Upper unit north HP
Type	Unbrushed	Unbrushed	Brushed	Brushed	Brushed	Brushed	Brushed	Brushed	Brushed
Sol #	749	750	754	763	764	1368	1432	1434	1453
wt.%									
SiO_2	45.2 (0.3)	45.3 (0.3)	45.4 (0.4)	46.0 (0.3)	46.6 (0.4)	46.4 (0.5)	45.1 (0.5)	45.1 (0.5)	45.8 (0.5)
TiO_2	0.74 (0.06)	0.67 (0.06)	1.01 (0.06)	0.93 (0.06)	1.11 (0.07)	0.97 (0.07)	0.97 (0.09)	1.02 (0.07)	1.04 (0.07)
Al_2O_3	8.9 (0.1)	7.9 (0.1)	9.3 (0.1)	9.3 (0.1)	10.0 (0.1)	9.2 (0.2)	9.2 (0.1)	9.1 (0.1)	9.1 (0.1)
FeO*	17.7 (0.1)	17.8 (0.1)	15.4 (0.1)	16.9 (0.1)	15.4 (0.1)	16.7 (0.1)	16.3 (0.1)	16.3 (0.1)	16.5 (0.1)
MnO	0.39 (0.01)	0.47 (0.01)	0.32 (0.01)	0.31 (0.01)	0.29 (0.01)	0.32 (0.01)	0.32 (0.01)	0.33 (0.01)	0.32 (0.01)
MgO	9.2 (0.1)	12.0 (0.1)	9.5 (0.1)	9.6 (0.1)	10.3 (0.1)	9.7 (0.2)	9.2 (0.1)	9.5 (0.1)	10.2 (0.2)
CaO	6.1 (0.0)	5.8 (0.0)	6.7 (0.0)	6.5 (0.0)	6.7 (0.0)	6.4 (0.1)	6.5 (0.1)	6.5 (0.1)	6.3 (0.1)
Na_2O	3.1 (0.2)	2.3 (0.2)	3.5 (0.2)	3.3 (0.2)	3.4 (0.2)	2.7 (0.4)	3.0 (0.3)	3.0 (0.3)	3.1 (0.3)
K_2O	0.32 (0.05)	0.23 (0.05)	0.42 (0.06)	0.21 (0.05)	0.32 (0.06)	0.26 (0.06)	0.35 (0.06)	0.33 (0.06)	0.29 (0.06)
P_2O_5	0.87 (0.07)	0.79 (0.07)	1.37 (0.07)	1.12 (0.07)	1.27 (0.08)	1.11 (0.08)	1.13 (0.08)	1.16 (0.08)	1.20 (0.08)
Cr_2O_3	0.45 (0.03)	0.49 (0.03)	0.32 (0.03)	0.39 (0.03)	0.34 (0.03)	0.34 (0.03)	0.36 (0.04)	0.39 (0.04)	0.38 (0.03)
SO_3	5.7 (0.1)	4.6 (0.1)	4.8 (0.06)	3.7 (0.05)	2.9 (0.05)	4.4 (0.1)	6.0 (0.1)	5.5 (0.1)	3.9 (0.1)
Cl	1.3 (0.0)	1.6 (0.0)	1.9 (0.0)	1.7 (0.0)	1.4 (0.0)	1.4 (0.0)	1.5 (0.0)	1.6 (0.0)	1.6 (0.0)
ppm									
Ni	317 (35)	352 (0.39)	379 (35)	318 (37)	297 (40)	359 (46)	404 (49)	333 (48)	382 (46)
Zn	400 (11)	415 (14)	407 (11)	422 (13)	314 (14)	480 (20)	402 (20)	408 (20)	391 (18)
Br	475 (17)	370 (18)	181 (15)	203 (16)	91 (15)	240 (20)	158 (20)	181 (20)	227 (20)

Target	Wendell_Pruit1	Wendell_Pruit2	Texas Chili_Brushed	Pesapallo	Superpesis	Elizabeth Emery	JuneEmerson	Esperanza
Section	Chanute	Chanute		Pesapallo	Pesapallo	Pesapallo	Pesapallo	
Location	Upper unit north HP	Upper unit north HP	Upper sfc. south HP	Upper unit east HP	Upper unit east HP	Upper unit east HP	Upper sfc. east HP	Low ridge basalt
Type	Brushed	Brushed	Brushed	Brushed	Brushed	Brushed	Brushed	Unbrushed
Sol #	1489	1491	1326	1206	1209	1216	1211	1055
wt.%								
SiO_2	45.7 (0.5)	45.7 (0.5)	45.2 (0.3)	46.8 (0.4)	46.0 (0.4)	46.2 (0.1)	46.7 (0.4)	47.9 (0.5)
TiO_2	1.10 (0.08)	1.06 (0.08)	1.04 (0.07)	1.20 (0.07)	1.01 (0.07)	0,90 (0.07)	0.86 (0.07)	1.05 (0.08)
Al_2O_3	9.4 (0.1)	9.4 (0.2)	9.4 (0.1)	10.2 (0.1)	10.0 (0.1)	9.7 (0.1)	9.8 (0.1)	8.4 (0.1)
FeO*	15.7 (0.1)	15.7 (0.1)	16.3 (0.1)	15.5 (0.1)	15.9 (0.1)	16.8 (0.1)	16.6 (0.1)	20.2 (0.2)
MnO	0.33 (0.01)	0.32 (0.01)	0.33 (0.01)	0.33 (0.01)	0.33 (0.01)	0.33 (0.01)	0.34 (0.01)	0.38 (0.01)
MgO	8.8 (0.1)	8.8 (0.2)	9.2 (0.1)	9.4 (0.1)	8.8 (0.1)	9.2 (0.2)	9.8 (0.1)	8.4 (0.1)
CaO	6.8 (0.1)	6.8 (0.1)	6.4 (0.0)	6.4 (0.1)	6.2 (0.0)	6.3 (0.0)	6.3 (0.1)	5.6 (0.1)
Na_2O	3.1 (0.2)	3.0 (0.3)	3.3 (0.2)	3.0 (0.2)	3.1 (0.3)	2.9 (0.3)	3.1 (0.3)	3.4 (0.3)
K_2O	0.38 (0.06)	0.39 (0.06)	0.44 (0.06)	0.46 (0.06)	0.43 (0.06)	0.40 (0.06)	0.43 (0.06)	0.52 (0.06)
P_2O_5	1.32 (0.09)	1.35 (0.09)	1.15 (0.07)	1.63 (0.08)	1.08 (0.08)	1.08 (0.08)	1.06 (0.08)	0.91 (0.08)
Cr_2O_3	0.34 (0.04)	0.32 (0.04)	0.32 (0.03)	0.33 (0.03)	0.31 (0.03)	0.42 (0.03)	0.45 (0.01)	0.20 (0.03)
SO_3	5.7 (0.1)	5.7 (0.1)	5.1 (0.1)	3.8 (0.1)	5.9 (0.1)	4.9 (0.1)	3.8 (0.1)	2.4 (0.1)
Cl	1.3 (0.0)	1.4 (0.0)	1.8 (0.0)	0.8 (0.0)	0.8 (0.0)	0.7 (0.01)	0.6 (0.02)	0.5 (0.02)
ppm								
Ni	381 (49)	339 (49)	349 (40)	478 (48)	420 (39)	362 (40)	310 (39)	395 (54)
Zn	463 (21)	435 (22)	566 (16)	680 (21)	570 (15)	568 (16)	471 (15)	368 (22)
Br	179 (20)	183 (20)	147 (16)	115 (16)	81 (15)	42 (15)	28 (15)	181 (23)

Results are calibrated according to Gellert et al. (2006) and are more fully presented by Ming et al. (2008). Values in parentheses are 2σ error. FeO* concentrations are total Fe as FeO. The valence state of S is unknown and is reported here as SO_3.

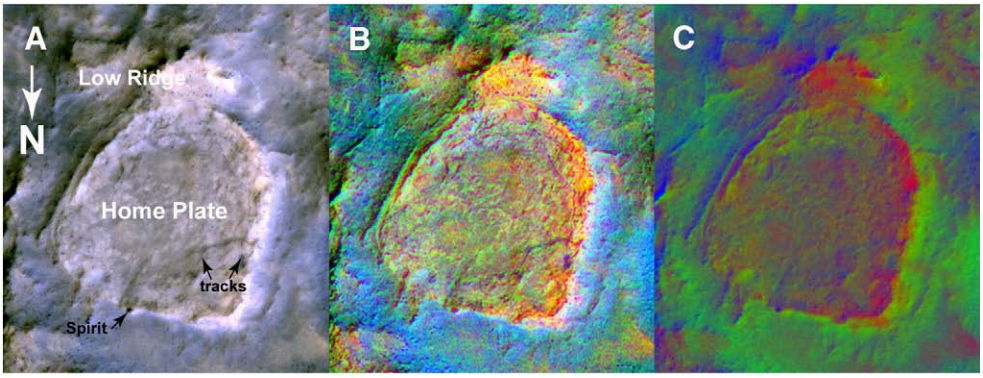

Fig. 3. A: False color HiRISE image of Home Plate, PSP_008963_1650 (collected 6/24/07) illustrating the near-infrared (874 nm), red (694 nm), and blue-green (536 nm) channels. B: Decorrelation stretch of HiRISE subscene. C: Composite of fraction images by spectral mixture analysis (Adams et al., 1993). Bright dust or bright colored surfaces are red, basaltic sands or spectrally similar materials are in green and shaded surfaces are blue. Images are more fully described in text.

different. The east side has more pyroxene, magnetite, and higher Al, Si/Mg, Zn, Ni, and K (e.g., Fig. 7A) whereas the west side has more olivine, npOx, and higher Cl and Br (e.g., Fig. 7B). VNIR spectral contrasts observed from orbit by HiRISE (Fig. 3), from the summit of Husband Hill by Pancam (Fig. 4A–B), and in 13-filter Pancam images of RAT brush spots (Fig. 5) are consistent with mineralogical observations and indicate that variations are continuous across Home Plate and are not limited to rocks examined *in situ*.

Compositional similarities in major elements along with geologic observations (Lewis et al., 2008) indicate that the upper, cross-bedded materials of Home Plate belong to the same stratigraphic unit. In contrast, mineralogy and compositions of the more fluid-soluble elements in the upper unit vary independently of stratigraphy.

Igneous processes (e.g., peritectic breakdown of olivine or quartz–fayalite–magnetite, QFM fO_2 buffer reaction) are difficult to envision causing the lateral variations within a single stratigraphic horizon over 80 m distance. An igneous origin for the magnetite in the Home Plate rocks was suggested by Morris et al. (2008) because Martian Shergottite–Nakhlite–Chassignite meteorites have igneous titanomagnetite and airfall dust captured by magnets on top of the rover contains titanomagnetite (Ming et al., 2008). While this may point to an igneous origin of the magnet-captured titanomagnetite, there is no compelling evidence that this dust was primarily derived from Home Plate. Airfall dust is globally homogeneous and not dominated by the composition of local rocks (Yen et al., 2005) and larger saltated particles, while more locally-derived, could come from any rock in Gusev Crater. Large-scale movement of dust and sand-sized particles has been an important process in the Inner Basin of the Columbia Hills, as evidenced by the existence of the ~0.3 km-wide El Dorado dune field ~0.5 km to the north (Sullivan et al., 2008). The upper unit of Home Plate at both the east and west sides has similar concentrations of Fe and Ti (Fig. 7A) but magnetite contents do vary (Fig. 4C). This indicates that there is no correlation between Ti concentrations and magnetite contents and that titanomagnetite accumulation or fractionation did not occur. Morris et al. (2008) rule out magnetite formed by serpentinization of olivine because MB did not detect Fe-bearing phyllosilicate minerals. But there are many other alteration mechanisms that form magnetite, including oxidizing, low fS_2 hydrothermal systems (e.g., Simon et al., 2004). Both igneous and secondary magnetite can be found in the same deposit, such as the Stardalur magnetic anomaly, Iceland, where anomalous concentrations of magnetite in Fe-rich basalts formed by the peritectitic breakdown of olivine and subsequent hydrothermal alteration (Vahle et al., 2007). While we cannot discount that magnetite at Home Plate may be igneous, a secondary origin as an alteration product is equally plausible.

Fe-bearing mineral contents at eastern Home Plate are similar to a nearby, vesicular basalt named Esperanza, which contains mainly pyroxene and magnetite and no significant olivine and npOx (Table 1). This resemblance might indicate that eastern Home Plate is unaltered, but it does not explain why stratigraphically equivalent rocks across Home Plate have different olivine contents. Eolian reworking of tephra deposits might concentrate higher density magnetite close to its source, but eolian processes would not fractionate olivine from pyroxene or account for variations among minor elements. We instead propose that variations across Home Plate reflect overprinting by both high and low temperature alteration.

5. Overprinting alteration of Home Plate

Mini-TES observations indicate that a component modeled as basaltic glass is abundant in western Home Plate rocks, but MB did not detect Fe-bearing glass (Tables 1 and 2; McSween et al., 2008; Morris et al., 2008). Glass is meta-stable and should either dissolve (Bandstra and Brantley, 2008) or devitrify at the martian surface over time (e.g., Lofgren, 1970). Devitrification of basaltic glass on Earth in the presence of water occurs by hydration and ion exchange to form palagonite, an assemblage of Fe-bearing clay and zeolite (Moore, 1966; Stroncik and Schmincke, 2002). Devitrification and hydration of basaltic glass at Mars surface condition instead forms npOx (e.g., Singer, 1982; Morris et al., 2001), which is abundant at Home Plate according to the MB (Table 1; Morris et al., 2008). Breakdown of basaltic glass to form npOx may have been caused by either chemical weathering (Morris et al., 2008) or by low temperature hydrothermal alteration (Schmidt et al., 2008). A correlation between npOx content and Cl concentration (Fig. 7F) for eastern Home Plate rocks supports the notion that devitrification and npOx formation is related to an influx of volatiles, such as a hydrothermal brine or vapor as suggested by Schmidt et al. (2008).

Olivine and glass will not persist for greater than 10^4–10^6 years if they are exposed to aqueous fluids, particularly at low pH and or higher temperatures (e.g., Stopar et al., 2006; Hausrath et al., 2008). But even at low temperature, olivine dissolution is a relatively rapid process at the surface of Mars under current cold, dry conditions, where ephemeral acidic fluids contribute to the dissolution of olivine (Hurowitz et al., 2006; Tosca et al., 2004). In the Gusev Plains, for example, Adirondack class basalt rock exteriors and soils have lower olivine contents than RAT-abraded rock interiors (Hurowitz et al., 2006; McSween et al., 2006). Importantly, the olivine found in Home Plate rocks reflects the primary igneous mineralogy, not a secondary assemblage. The occurrence of olivine

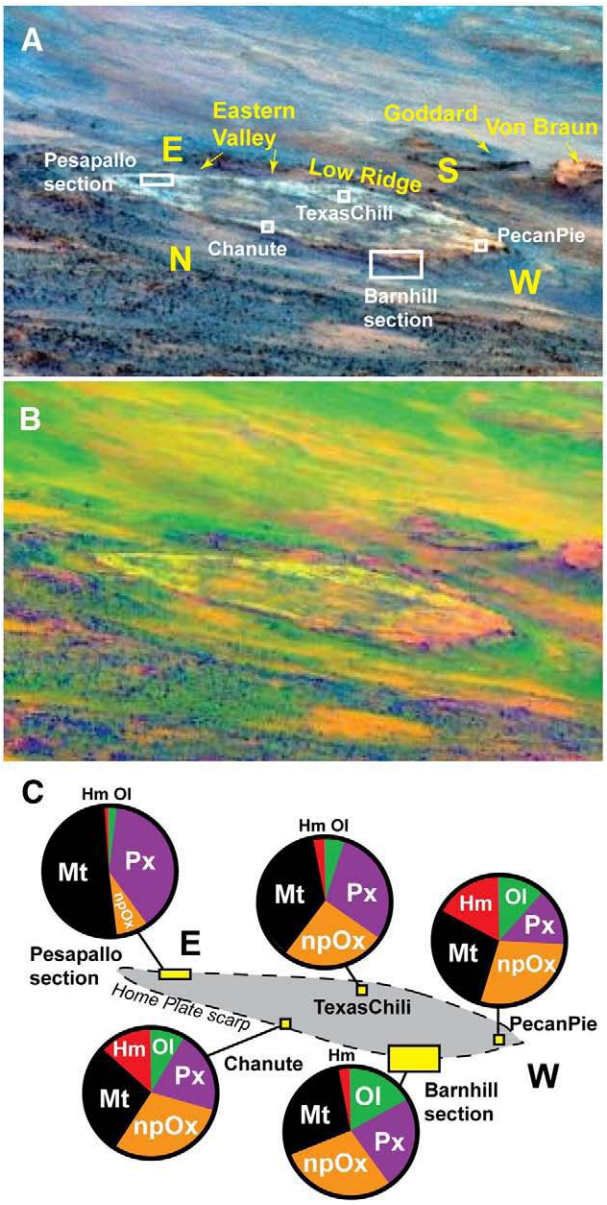

Fig. 4. A: False color Pancam image of Home Plate from the summit of Husband Hill. RGB = 753, 535, 432 nm. B: Composite of A where red is the slope between 436 and 754 nm reflectance values, green is 436 nm reflectance and blue is the slope between the 754 nm and 1009 nm reflectance values. C: Series of pie charts indicating relative abundances of Fe-minerals around the perimeter of Home Plate. Ol olivine, Px pyroxene, Mt magnetite, Hm hematite (Table 1).

on the west side (Table 1) probably indicates that aqueous fluids never persistently saturated those rocks. Basaltic glass is found in the east according to deconvolutions of the Mini-TES data (~20%; Table 2), but analogous npOx is not identified in the MB observations. The Fe component in the basaltic glass may have instead devitrified to form magnetite.

The near absence of olivine as seen by the MB at eastern Home Plate indicates either that aqueous fluids dissolved it or that it recrystallized to yield pyroxene and magnetite. Variations in MgO and SiO_2 from west to east could result from mass-balanced removal of 2–6% olivine (Fig. 7B), but this does not account for the near constant sum of pyroxene and olivine across Home Plate. Symplectic oxidation of olivine at T>~500 °C may also produce magnetite and low-Ca pyroxene with Fe-contents dependent on the fO_2 and the initial Fe in the olivine ($3Fe_2SiO_4 + O_2 \rightarrow 2Fe_3O_4 + 3SiO_2$, where SiO_2 combines with Mg or Fe to form pyroxene). This high temperature reaction has been suggested to explain lower olivine contents in rock interiors than exteriors in the Gusev Plains basalts (Gunnlaugsson et al., in press), but would result in a net loss of the sum of Fe in olivine and pyroxene (Haggerty and Baker, 1967). The Fe in olivine at the eastern side of Home Plate was more likely converted to pyroxene through the addition of SiO_2 by a localized, subsolidus peritectic reaction or via a late-stage fluid combined with symplectic oxidation ($Fe_2SiO_4 + SiO_2 \rightarrow 2FeSiO_3$). This processes is supported by a correlation between pyroxene and SiO_2 concentration (Fig. 7E) excluding hematite-rich Pecan Pie. Hematite in Pecan Pie correlates with lower total pyroxene and olivine than other Home Plate targets, suggesting enhanced alteration of these Fe silicates at this site. The process of silica addition to olivine to form pyroxene has been identified in some martian Nahklite meteorites (Treiman, 2005; Trieman and Irving, in press).

Mass transfer during the recrystallization event is implied by small but systematic changes in composition across Home Plate (Fig. 7B–D). Under hydrothermal conditions, SiO_2 is more soluble and Zn and Ni can form chloride complexes whose stability correlates strongly with temperature (0–300 °C; Sverjensky et al., 1997). Because higher Si/Mg, Zn, and Ni concentrations are observed in eastern Home Plate rocks, higher temperatures likely were attained there. The localized nature of the high temperature alteration suggests the event was relatively short-lived and temperature gradients were steep, possibly caused by a nearby dike injection or influx of volcanic gas. Because no pyrite or Fe-sulfates have been identified in Home Plate rocks by the MB, the influx of heat that altered eastern Home Plate was probably associated with a sulfur-poor fluid or vapor. Acid sulfate vapors have been significant alteration agents elsewhere in the vicinity of Home Plate, such as for hydrated Fe-sulfate soils Tyrone (Yen et al., 2008) and the pyrite/marcasite-bearing float rock FuzzySmith (Squyres et al., 2007). The heterogeneous distribution of these deposits indicates that alteration conditions varied in time and space and may have involved the boiling and fractionation of an acid sulfate vapor from a Cl-rich brine at depth (Schmidt et al., 2008). Although volatile and soluble elements, such as Zn and Cl were mobile, ambient water pressures were probably low because no clays or other hydrated minerals have been detected. Lateral advection was probably minor across Home Plate and thus conduction was the main mode of heat transport.

The high and low temperature alteration events at Home Plate may or may not be temporally related to one another, and putting the

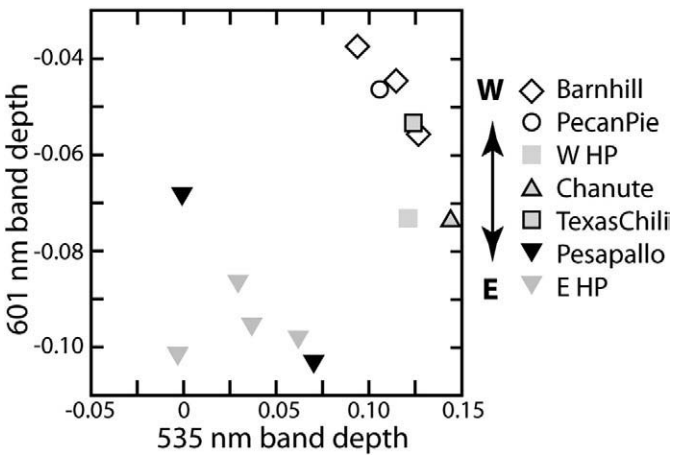

Fig. 5. Plot of 601 vs. 535 nm band depths from Pancam images of RAT brush spots (Fig. 1) and relatively dust-free rock surfaces from west and east Home Plate (W HP and E HP, respectively).

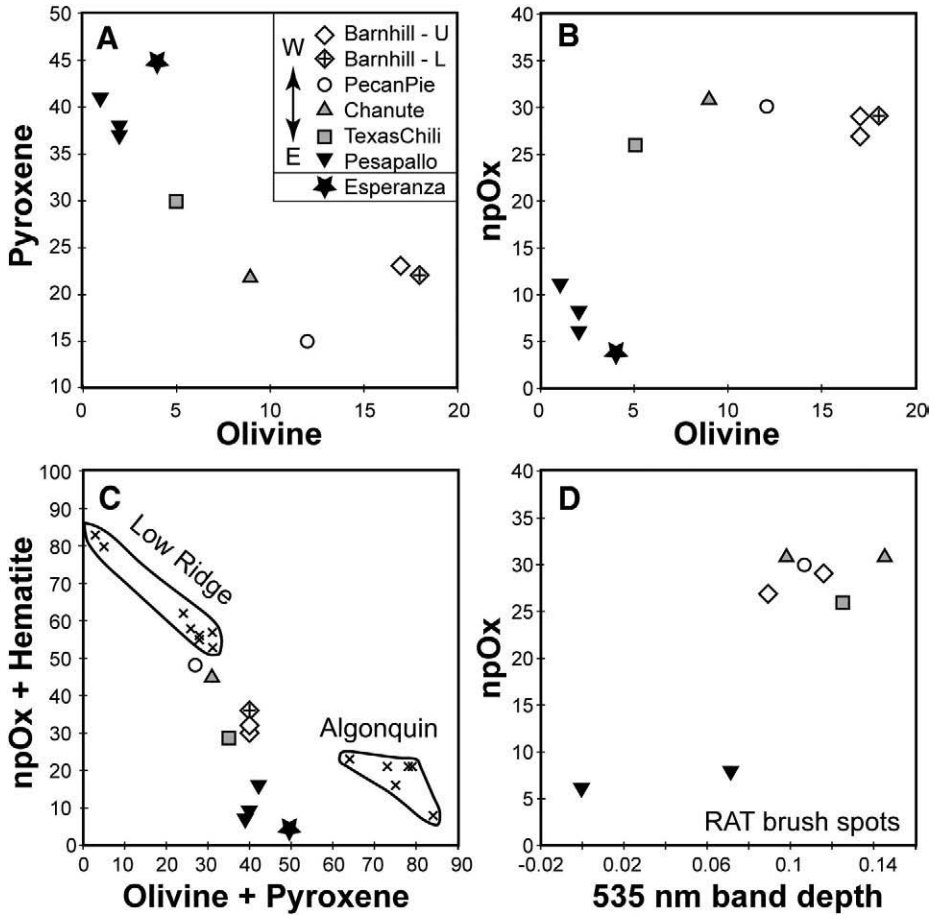

Fig. 6. Variation diagrams of subspectral areas for Fe-bearing minerals derived by MB of Home Plate rocks and a nearby vesicular basalt called Esperanza (Table 1). A: Pyroxene vs. Olivine. B: NpOx vs. Olivine. C: Sum of subspectral areas of npOx and hematite vs. the sum of the subspectral areas of olivine and pyroxene for Home Plate rocks. Also shown are the hematite-rich layered tephras of Low Ridge and the ultramafic clastic Algonquin rocks from the north side of the Inner Basin of the Columbia Hills (Morris et al., 2008). D: NpOx vs. the 535 nm band depth from the Pancam spectra of the RAT brush spot. Note that the MB samples a greater depth of the rock (~200 μm) than the Pancam (0–2 μm).

alteration of Home Plate in context with other altered rocks is complicated by uncertainties in relative timing of deposition and alteration. Some layered tephra deposits located to the south of Home Plate at Low Ridge (Fig. 1) have been found with very high Zn (up to 2300 ppm), Ni (up to 2000 ppm) and K_2O (up to 3 wt.%) as well as very high hematite contents (Ming et al., 2008; Morris et al., 2008). These rocks may share a common protolith with Home Plate (Ming et al., 2008) and probably experienced even higher temperatures and more oxidizing conditions than eastern Home Plate. Other altered rocks include light-toned Mg-rich, Al-poor outcrops called Everett and Slide, located several meters east of Home Plate in the Eastern Valley (Ming et al., 2008). Everett and Slide contain an assemblage of magnetite>pyroxene>npOx (Morris et al., 2008) and have high Zn (up to 1340 ppm) and Ni (up to 850 ppm; Ming et al., 2008). These outcrops may have experienced similar high temperature alteration to the east side of Home Plate, but their protolith and stratigraphic position are unknown.

The presence of high silica deposits of hydrothermal origin in the Eastern Valley is intriguing and may imply a petrogenic link (Fig. 1; Squyres et al., 2008). But the relationship of the silica deposits with the higher temperature alteration of eastern Home Plate is not clear because their lateral extent is unknown and they may be a stratigraphically lower layer, discontinuous altered pods, or late sinter deposits. Models for the silica deposition will be tested as Spirit explores the areas away from Home Plate. Nevertheless, the sheer diversity of alteration regimes over a small area (<0.01 km^2) suggests a dynamic, laterally variable hydrothermal system once existed around Home Plate.

6. Conclusions

The coherent spectral, mineralogical, and geochemical variations across Home Plate record two discrete alteration regimes: a localized, high temperature event that affected the east side, and a lower temperature alteration that formed npOx at the west. The relative timing of the two alteration events is unknown. Other altered deposits have been identified in Gusev Crater (e.g., Ming et al., 2006; Haskin et al., 2005) and, in the Home Plate region, higher temperatures and greater degrees of alteration are inferred (Ming et al., 2008; Squyres et al., 2008). But Spirit's quasi-circular traverse at Home Plate has allowed us to incorporate spatial data over a continuous rock unit and to begin to envision scenarios of lateral heat and fluid flow.

Acknowledgements

Funding for Athena science team members was provided by NASA Mars Exploration Rover mission contracts through the Jet Propulsion Laboratory. This manuscript was improved by reviews on a previous version by Joshua Bandfield and two anonymous reviewers and three anonymous reviewers on the current incarnation. We thank the HiRISE team for making their high quality images of Mars available to

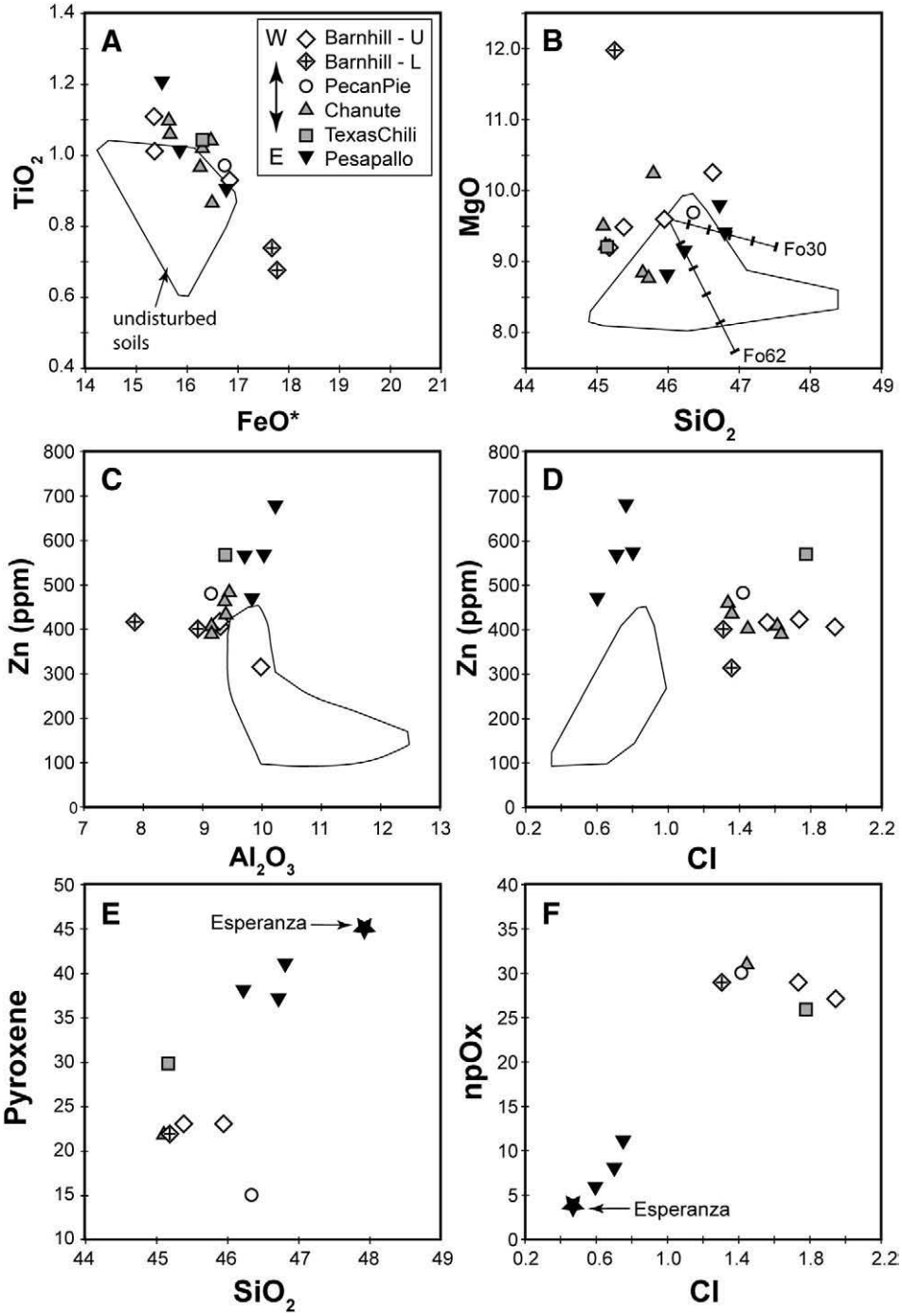

Fig. 7. Major and minor element variation diagrams of Home Plate rock targets. U and L are upper and lower Barnhill, respectively. All targets were RAT brushed, except Barnhill-L. Fields indicate ranges in compositions of undisturbed Gusev soils, a likely dust contaminant. Units are wt.% unless noted. For simplicity, error bars for the elemental data are not presented, but their uncertainty is included in Table 3. A: TiO_2 vs. total Fe as FeO*B: MgO vs. SiO_2. Mass balanced olivine dissolution trends (Fo30, Fo62) from a Barnhill target have tics indicating 2% olivine removal. C: Zn vs. Al_2O_3 D: Zn vs. Cl E: Subspectral area of pyroxene derived from MB (Table 1) vs. SiO_2 F: Subspectral area of npOx derived by MB (Table 1) vs. Cl.

the scientific community. And we especially thank the team of scientists and engineers who have made and who continue to make Mars Rover science so successful.

References

Adams, J.B., Smith, M.O., Gillespie, A.R., 1993. Imaging spectroscopy: interpretation based on spectral mixture analysis. In: Pieters, C.M., Englert, P.A.J. (Eds.), Remote Geochemical Analysis: Elemental and Mineralogical Composition. Cambridge University Press, New York, pp. 145–166.

Arvidson, R.E., et al., 2008. Spirit Mars rover mission to the Columbia Hills, Gusev Crater: mission overview and selected results from Cumberland Ridge to Home Plate. J. Geophys. Res. 113, E12S33. doi:10.1029/2008JE003183.

Bandstra, J.Z., Brantley, S.L., 2008. Data fitting techniques with applications to mineral dissolution kinetics. In: Brantleyet al. et al., S.L. (Ed.), Kinetics of Water–rock Interactions. Springer, New York, pp. 211–258.

Farrand, W.H., Bell III, J.F., Johnson, J.R., Squyres, S.W., Soderblom, J., Ming, D.W., 2006. Spectral variability among rocks in visible and near-infared multispectral Pancam data collected at Gusev Crater: examinations using spectral mixture analysis and related techniques. J. Geophys. Res. 111, E02S15. doi:10.1029/2005JE002495.

Farrand, W.H., Bell III, J.F., Johnson, J.R., Arvidson, R.E., Crumpler, L.S., Hurowitz, J.A., Schröder, C., 2008. Rock spectral classes observed by the Spirit rover's Pancam on

the Gusev crater plains and in the Columbia Hills. J. Geophys. Res. 113, E12S38. doi:10.1029/2008JE003237.
Gellert, R., Rieder, R., Brückner, J., Clark, B., Dreibus, G., Klingelhöfer, G., Lugmair, G., Ming, D., Wänke, H., Yen, A., Zipfel, J., Squyres, S.W., 2006. Alpha Particle X-ray Spectrometer (APXS): results from Gusev Crater and calibration report. J. Geophys. Res. 111, E02S05. doi:10.1029/2005JE002555.
Gunnlaugsson, H.P., Rasmussen, H., Madsen, M.B., Nørnberg, P., in press. New analysis of the Mössbauer spectra of olivine basalt rocks from Gusev crater on Mars, Planet. Space Sci.
Haggerty, S.E., Baker, I., 1967. The alteration of olivine in basaltic and associated lavas — Part I: high temperature alteration, Contrib. Mineral. Petrol. 16, 233–257.
Haskin, L.A., et al., 2005. Water alteration of rocks and soils on Mars at the Spirit rover site in Gusev Crater. Nature 436, 66–69. doi:10.1038/nature03640.
Hausrath, E.M., Navarre-Stichler, A.K., Sak, P.B., Steefel, C.I., Brantley, S., 2008. Basalt weathering rates on Earth and the duration of liquid water on the plains of Gusev Crater, Mars. Geology 36, 67–70.
Hurowitz, J.A., McLennan, S.M., Tosca, N.J., Arvidson, R.E., Michalski, J.R., Ming, D.W., Schröder, C., Squyres, S., 2006. In situ and experimental evidence for acidic weathering of rocks and soils on Mars. J. Geophys. Res. 111, E02S19. doi:10.1029/2005JE002515.
Lewis, K.W., Aharonson, O., Grotzinger, J.P., Squyres, S.W., Schmidt, M.E., Bell, J.F., Crumpler, L.S., 2008. Structure and stratigraphy of Home Plate from the Spirit Mars Exploration Rover, J. Geophys. Res., 113, E12S36, doi:10.1029/2007JE003025.
Lofgren, L., 1970. Experimental devitrification of rhyolite glass. Geol. Soc Am. Bull. 81, 553–559.
McEwen, A.S., Eliason, E.M., Bergstrom, J.W., Bridges, N.T., Hansen, C.J., Delamere, W.A., Grant, J.A., Gulick, V.C., Herkenhoff, K.E., Keszthelyi, L., Kirk, R.L., Mellon, M.T., Squyres, S.W., Thomas, T., Weitz, C., 2007. Mars Reconnaissance Orbiter's High Resolution Imaging Science Experiment (HiRISE). J. Geophys. Res. 112, E12001. doi:10.1029/2007JE002925.
McSween, H.Y., et al., 2006. Characterization and petrologic interpretation of olivine-rich basalts at Gusev Crater. J. Geophys. Res. 111, E02S10. doi:10.1029/2005JE002698.
McSween, H.Y., Ruff, S.W., Morris, R.V., Gellert, R., Klingelhöfer, G., Christensen, P.R., McCoy, T.J., Ghosh, A., Moersch, J.M., Cohen, B.A., Rogers, A.D., Schröder, C., Squyres, S.W., Crisp, J., Yen, A., 2008. Mineralogy of volcanic rocks in Gusev Crater, Mars: reconciling Mössbauer, APXS, and Mini-TES spectra. J. Geophys. Res. 113, E06S04. doi:10.1029/2007JE002970.
Ming, D.W., Mittlefehldt, D.W., Morris, R.V., Golden, D.C., Gellert, R., Yen, A., Clark, B.C., Squyres, S.W., Farrand, W.H., Ruff, S.W., Arvidson, R.E., Klingelhöfer, G., McSween, H. Y., Rodionov, D.S., Schröder de Souza, P.A., Wang, A., 2006. Geochemical and mineralogical indicators for aqueous processes in the Columbia Hills of Gusev Crater, Mars. J. Geophys, Res. 111, E02S12. doi:10.1029/2005JE002560.
Ming, D.W., Gellert, R., Morris, R.V., Arvidson, R.E., Brückner, J., Clark, B.C., Cohen, B.A., D, Uston, C., Economou, T., Fleischer, I., Klingelhöfer, G., McCoy, T.J., Mittlefehldt, D.W., Schmidt, M.E., Schröder, C., Squyres, S.W., Tréguier, E., Yen, A.S., Zipfel, J., 2008. Geochemical properties of rocks and soils in Gusev Crater, Mars: results of the Alpha Particle X-Ray Spectrometer from Cumberland Ridge to Home Plate. J. Geophys. Res. 113, E12S39. doi:10.1029/2008/JE003195.
Moore, J.G., 1966, Rate of palagonization of submarine basalt adjacent to Hawaii, D163-71, U.S. Geol. Survey Prof. Paper, 550-D.
Morris, R.V., Golden, D.C., Ming, D.W., Shlfer, T.D., JØrgensen, L.C., Bell III, J.F., Graff, T.G., Mertzman, S.A., 2001. Phyllosilicate-poor palagonitic dust from Mauna Kea Volcano (Hawaii): a mineralogical analogue for magnetic Martian dust? J. Geophys. Res. 106 (E3), 5057–5083.
Morris, R.V., Klingelhöfer, G., Schröder, C., Fleischer, I., Ming, D.W., Yen, A.S., Gellert, R., Arvidson, R.E., Rodionov, D.S., Crumpler, L.S., Clark, B.C., Cohen, B.A., McCoy, T.J., Mittlefehldt, D.W., Schmidt, M.E., de Souza Jr., P.A., Squyres, S.W., 2008. Iron mineralogy and aqueous alteration from Husband Hill through Home Plate at Gusev Crater, Mars: results from the Mössbauer instrument on the Spirit Mars Exploration Rover. J. Geophys. Res. 113, E12S42. doi:10.1029/2008JE003201.
Ruff, S.W., Christensen, D.L., Blaney, D.L., Farrand, W.H., Johnson, J.R., Michalski, J.R., Moersch, J.E., Wright, S.P., Squyres, S.W., 2006. The rocks of Gusev Crater as viewed by the Mini-TES instrument. J. Geophys. Res. 111, E12S18. doi:10.1029/2006JE002747.
Schmidt, M.E., Ruff, S.W., McCoy, T.J., Farrand, W.H., Johnson, J.R., Gellert, R., Ming, D.W., Morris, R.V., Cabrol, N., Lewis, K.W., Schröder, C., 2008. The hydrothermal origin of halogens at Home Plate, Gusev Crater. J. Geophys. Res. 113, E06S12. doi:10.1029/2007JE003027.
Schröder, C., Di, K., Morris, R.V., Klingelhöfer, G., Li, R., 2008. An east to west mineralogical trend in Mars Exploration Rover Spirit Mössbauer spectra of Home Plate. Lunar Planet. Sci. XXXIX, abs# 2153.
Simon, A.C., Pettke, T., Candela, P.A., Piccoli, P.M., Heinrich, C.A., 2004. Magnetite solubility and iron transport in magmatic-hydrothermal environments. Geochim. Cosmochim. Acta 68, 4905–4914. doi:10.1016/j.gca.2004.05.033.
Singer, R.B., 1982. Spectral evidence for the mineralogy of high-albedo soils and dust on Mars. J. Geophys. Res. 87 (B12), 10,159–10,168.
Smith, M.D., Wolff, M.J., Spanovich, N., Ghosh, A., Banfield, D., Christensen, P.R., Landis, G.A., Squyres, S.W., 2006. On Martian year of atmospheric observations using MER Mini-TES. J. Geophys. Res. 111, E12S13. doi:10.1029/2006JE002770.
Squyres, S.W., Arvidson, R.E., Baumgartner, E.T., Bell, J.F., Christensen, P.R., Gorevan, S., Herkenhoff, K.E., Klingelhöfer, G., Madsen, M.B., Morris, R.V., Rieder, R., Romero, R. A., 2003. The Athena Mars rover science investigation. J. Geophys. Res. 108 (E12), 8063. doi:10.1029/2003JE002121.
Squyres, S.W., et al., 2007. Pyroclastic activity at Home Plate in Gusev Crater, Mars. Science 316, 738–742.
Squyres, S.W., Arvidson, R.E., Ruff, S., Gellert, R., Morris, R.V., Ming, D.W., Crumpler, L., Farmer, J.D., Des Marais, D.J., Yen, A., McLennan, S.M., Calvin, W., Bell III, J.F., Clark, B. C., Wang, A., McCoy, T.J., Schmidt, M.E., de Souza, P.A., 2008. Detection of silica-rich deposits on Mars. Science 320, 1063–1067.
Stopar, J.D., Taylor, G.J., Hamilton, V.E., Browning, L., 2006. Kinetic model of olivine dissolution and extent of aqueous alteration on Mars. Geochim. Cosmochim. Acta 70, 6136–6152.
Stroncik, N.A., Schmincke, H.U., 2002. Palagonite — a review. Intl. J. Earth Sci. 91, 680–697.
Sullivan, R., Arvidson, R., Bell III, J.F., Gellert, R., Golombek, M., Herkenhoff, K., Johnson, J., Thompson, S., Whelley, P., Wray, J., 2008. Wind-driven particle mobility on Mars: insights from Mars Exploration Rover observations at "El Dorado" and surroundings at Gusev Crater. J. Geophys. Res. 113, E06S07. doi:10.1029/2008JE003101.
Sverjensky, D.A., Shock, E.L., Helgeson, H.C., 1997. Prediction of the thermodynamic properties of aqueous metal complexes to 1000 °C and 5 kb. Geochim. Cosmochim. Acta 61, 1359–1412.
Treiman, A.H., 2005. The nahklite martian meteorites: augite-rich igneous rock from Mars. Chem. Erde 65, 203–270.
Trieman, A.H., Irving, A.J., in press. Petrology of Martian meteorite Northwest Africa 998, Meteor. Planet. Sci., 43.
Tosca, N.J., McLennan, S.M., Lindsley, D.H., Schoonen, M.A.A., 2004. Acid sulfate weathering of synthetic Martian basalt: the acid fog model revisited. J. Geophys. Res. 109, E05003. doi:10.1029/2003JE002218.
Tosca, N.J., McLennan, S.M., Clark, B.C., Grotzinger, J.P., Hurowitz, J.A., Knoll, A.H., Schröder, C., Squyres, S.W., 2005. Geochemical modeling of evaporation processes on Mars: insight from the sedimentary record at Meridiani Planum. Earth Planet. Sci. Lett. 240, 122–148.
Vahle, C., Kotney, A., Gunnlaugsson, H.P., Kristjansson, L., 2007. The Stardalur magnetic anomaly revisited — new insights into a complex cooling and alteration history. Phys. Earth Planet. Inter. 164, 119–141. doi:10.1016/j.pei.2007.06.004.
Yen, A.S., et al., 2005. An integrated view of the chemistry and mineralogy of martian soils. Nature 436, 49–54. doi:10.1038/nature03637.
Yen, A.S., Morris, R.V., Clark, B.C., Gellert, R., Knudsen, A.T., Squyres, S., Mittlefehldt, D. W., Ming, D.W., Arvidson, R., McCoy, T., Schmidt, M., Hurowitz, J., Li, R., Johnson, J.R., 2008. Hydrothermal processes at Gusev Crater: an evaluation of Paso Robles class soils. J. Geophys. Res. 113, E06S10. doi:10.1029/2007JE002978.